ACS APPLIED MATERIALS & INTERFACES

Research Article

www.acsami.org

From Nanofibrillar to Nanolaminar Poly(butylene succinate): Paving the Way to Robust Barrier and Mechanical Properties for Full-Biodegradable Poly(lactic acid) Films

Lan Xie,[†,‡] Huan Xu,[†] Jing-Bin Chen,[†] Zi-Jing Zhang,[†] Benjamin S. Hsiao,[§] Gan-Ji Zhong,*[,†] Jun Chen,[†] and Zhong-Ming Li*[,†]

[†]State Key Laboratory of Polymer Materials Engineering, College of Polymer Science and Engineering, Sichuan University, Chengdu, 610065 Sichuan, People's Republic of China

[‡]Department of Materials Science and Engineering, University of Sheffield, Sheffield S1 3JD, United Kingdom

[§]Department of Chemistry, Stony Brook University, Stony Brook, New York 11794-3400, United States

Supporting Information

ABSTRACT: The traditional approach toward barrier property enhancement of poly(lactic acid) (PLA) is the incorporation of sheet-like fillers such as nanoclay and graphene, unfortunately leading to the sacrificed biocompatibility and degradability. Here we unveil the first application of a confined flaking technique to establish the degradable nanolaminar poly(butylene succinate) (PBS) in PLA films based on PLA/PBS in situ nanofibrillar composites. The combination of high pressure (10 MPa) and appropriate temperature (160 °C) during the flaking process desirably enabled sufficient deformation of PBS nanofibrils and retention of ordered PLA channels. Particularly, interlinked and individual nanosheets were created in composite films containing 10 and 20 wt % PBS, respectively, both of which presented desirable alignment and large width/thickness ratio (nanoscale thickness with a width of 428 ± 13.1 and 76.9 ± 8.2 μm, respectively). With the creation of compact polymer "nano-barrier walls", a dramatic decrease of 86% and 67% in the oxygen permeability coefficient was observed for the film incorporated with well-organized 20 wt % PBS nanosheets compared to pure PLA and pure PBS (1.4 and 0.6 × 10^{-14} $cm^3 \cdot cm \cdot cm^{-2} \cdot s^{-1} \cdot Pa^{-1}$), respectively. Unexpectedly, prominent increases of 21% and 28% were achieved in the tensile strength and modulus of composite films loaded 20 wt % PBS nanosheets compared to pure PLA films, although PBS intrinsically presents poor strength and stiffness. The unusual combination of barrier and mechanical performances established in the fully degradable system represent specific properties required in packaging beverages, food and medicine.

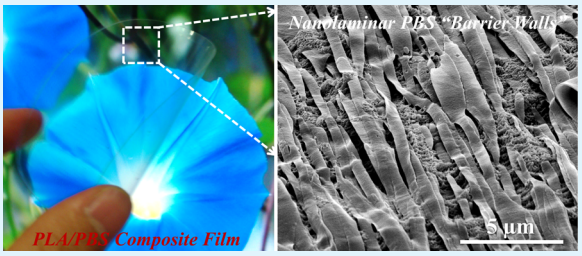

KEYWORDS: *full-degradable poly(lactic acid) film, poly(butylene succinate) nanolaminae, gas permeability, mechnical properties*

INTRODUCTION

The up-to-date development of biopolymer science and technology has generated a demand for the enhancement of functional properties (e.g., high thermal and electrical conductivity, low gas permeability) for an array of appealing applications.[1−8] One of the most typical and visible is the pursuit of multifunctional poly(lactic acid) (PLA): PLA has a great reputation among the emerging bioplastics in terms of desirable renewability,[9−12] impressive mechanical performance and outstanding biodegradability,[13−17] but the poor resistance to gas/water largely blocks its promising applications for green packaging.[18,19] As a result, the enhancement of gas barrier performance for PLA has prompted rapidly increasing efforts during the past decade, with the ultimate goal of substituting traditional petroleum-based products that currently dominate the packaging field.[20,21] Among the available approaches appearing in the recent progress, incorporating sheet-like nanofillers, such as nanoclay, graphene oxide, and their derivatives, into PLA is perceived as the common route to fabricate high barrier PLA composites.[22−25] Specifically, these introduced impermeable nanoplatelets are generally recognized as "nano-barrier walls", compelling the diffusing molecules to follow longer and more tortuous pathways.[26,27] An imperative task in preparing high barrier nanocomposites is to uniformly disperse and orderly organize the nanoplatelets in the polymeric matrix, and thus to translate competently the unique properties of individual nanoplatelets to larger scales.[28−30] It is pertinent to point out that, at present, time/energy-consuming efforts are normally engaged, such as surface decoration of the nanofillers,[31] complex processing technique or laboratory-scale production.[26] Of vital weakness is the sacrificed biocompatibility and biodegradability of PLA composites after introducing

Received: January 14, 2015
Accepted: March 31, 2015
Published: March 31, 2015

DOI: 10.1021/acsami.5b00294
ACS Appl. Mater. Interfaces 2015, 7, 8023−8032

nanofillers, depriving of the potential for packaging beverage, food and medicine.[20] It seems a continuing challenge to achieve simultaneously superior barrier properties and desirable degradability for PLA, especially during an industrially feasible manufacturing process.

Pioneering exploration in immiscible blends of polyamides or polyesters in the polyolefine matrix, particularly polyethylene, manifested that constructing parallel, thin and large laminae of dispersed phase during the blowing and extrusion molding substantially reduced the permeability properties (3−100 times).[32−35] And this methodology has been applied for commercial production of bottles and films since the late 1990s.[35] It naturally encourages us to extend the concept of functional laminar phase formation to manufacture PLA composites containing highly aligned laminar biopolymer, targeting full biodegradability and desirable barrier properties. However, to date, the exploitation of all-biopolymer blends featuring micro/nanosheet-like dispersed phase is still in its infancy, and almost none of the obvious opportunities to promoting the permeability resistance by establishing in situ nanosheets in biopolymers have been examined. Our recent exploration demonstrates the possibility to construct in situ nanofibrillar poly(butylene succinate) (PBS) utilizing intense extrusion compounding followed by "slit die extrusion-hot stretching-quenching" technique, permitting the nanofibrillation of nanosized PBS droplets in the PLA matrix.[36] Here we attempt to further tailor the morphology of PBS nanofibrils, i.e., establishing highly oriented PBS nanosheets by confined flaking of in situ nanofibrillar composites during the compression molding process, which is schematically depicted in Figure 1. The key element in this methodology is the application of appropriate molding temperature (160 °C), allowing the preservation of oriented units and sufficient thermal deformation of PBS nanofibrils but partial melting of PLA matrix. Moreover, the woven design may help build biaxial structures for the composite films rather than the anisotropic alignment of functional units, which is in great need for packaging, energy and transport-related applications.

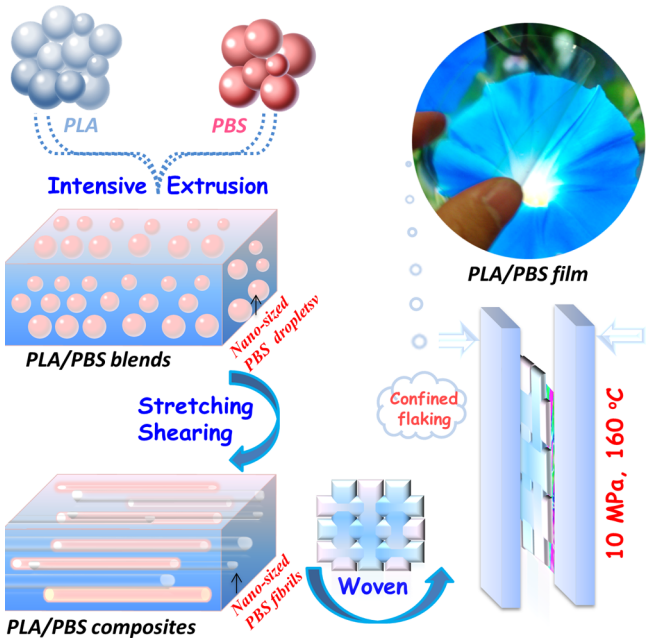

Figure 1. Schematic representation describing the processing approach for structuring the PLA/PBS films. Starting from the direct extrusion compounding of PLA and PBS, the PLA composites containing PBS nanofibrils are manufactured employing the "slit die extrusion-hot stretching-quenching" technique.[36] Subsequently, the composite sheets are woven into ordered platelets and finally, PLA/PBS composite films with a thickness of ∼100 μm are obtained by confined flaking at the specific temperature of 160 °C. It is worth noting that a woven structure is applied to preserve the oriented units by minimizing the random flow during confined flaking and to achieve the isotropic structure and performances, while the molding temperature is fixed at 160 °C to allow the sufficient thermal deformation of PBS nanofibrils but partial melting of PLA matrix. The digital photograph presents the appearance for the PLA/PBS (80/20) film, demonstrating high transparence and desirable toughness.

EXPERIMENTAL SECTION

Materials. PLA under a trade name of 4032D comprising ∼2% D-LA was commercially purchased from NatureWorks (USA), its weight-average and number-average molecular weight are 2.23×10^5 and 1.06×10^5 g/mol, respectively. PBS (Bionolle #1001MD) with a number-average molecular weight of $\sim 6.0 \times 10^4$ g/mol and a dispersive index of 2.33 was obtained from SHOWA Highpolymer Co. Ltd. (Japan).

Preparation of PLA/PBS Composite Films. Figure 1 depicts the confined flaking manufacture of PLA/PBS films based on PLA/PBS nanofibrillar composites. The nanofibrillar composites were woven into platelets and then submitted to compression molding at 160 °C under a fixed pressure of 10 MPa. Such a confined flaking process was hypothesized to desirably control phase morphology for nanofibrillar composites.[37] At this particular temperature (between the melting points of PBS and PLA), the semisolid, aligned tiny channels established by PLA largely confined the flow mobility of PBS which melts in the channels instead of direct fracture or relaxation of fibrillar PBS phase. Once subjected to high pressure, the PLA channels were compelled to generate sufficient, ordered deformation rather than disordered, overlapping integration, which triggered the structural alteration into nanolaminae from nanofibrils for PBS. For the sake of briefness, the detailed procedures of nanofibrillar composite preparation are not stated here, which were available in our recent work.[36]

Scanning Electronic Microscopy (SEM). Cryogenic fracture followed by selective etching of PLA matrix in dichloromethane (CH_2Cl_2) at 5 °C for 40 s was applied to obtain the specific surfaces showing the phase morphology for PBS. The surfaces sputter-coated with gold were observed with a field-emission SEM instrument (Inspect F, FEI, Finland) with an accelerated voltage of 10 kV.

Two-Dimensional Small-Angle X-ray Scattering (2D-SAXS). 2D-SAXS measurements were performed at the beamline BL16B1 of Shanghai Synchrotron Radiation Facility (SSRF, Shanghai, China). The monochromated X-ray beam operated at a wavelength of 0.124 nm with a beam size of 80 × 80 μm (length × width), and the sample-to-detector distance was fixed at 1900 mm. All the film samples (∼100 μm) were exposed to the X-ray for a fixed duration of 90 s. The 2D-SAXS images were collected with an X-ray CCD detector (Model Mar165, a resolution of 2048 × 2048 pixels). The radically integrated intensities $I(q)$ ($q = 4\pi\sin\theta/\lambda$) are obtained for integration in the azimuthal angular range of a whole circle, where 2θ stands for the scattering angle and λ represents the X-ray wavelength. And the long period (L) regarding the lamellar structure was calculated using the Bragg equation, $L = 2\pi/q^*$.

Two-Dimensional Wide-Angle X-ray Diffraction (2D-WAXD). 2D-WAXD determination was carried out at the beamline BL15U1 of SSRF, Shanghai. The monochromated X-ray beam with a wavelength of 0.124 nm was focused to an area of 3 × 2.7 μm (length × width), and the sample-to-detector distance from was set as 185 mm. After 90 s of exposure to the X-ray for the film samples (∼100 μm), the 2D-WAXD images were collected with an X-ray CCD detector (Model SX165, Rayonix Co. Ltd., USA). Additionally, the WAXD intensity profiles for each 2θ were obtained by integration in the azimuthal angular range of a whole circle (0−360°) from the sample patterns employing the Fit2D package, while background scattering was

DOI: 10.1021/acsami.5b00294
ACS Appl. Mater. Interfaces 2015, 7, 8023−8032

subtracted from the sample patterns. The orientation parameter of PLA matrix was calculated using Picken's method based on the reflection of lattice planes (200)/(110) of PLA α-form crystals, which enabled the quantitative evaluation of the order of molecular alignment.[38]

Differential Scanning Calorimetry (DSC). Pure PLA and composite films (around 5−6 mg) were heated from 30 to 200 °C on a DSC Q200 (TA Instruments, USA) at a heating rate of 10 °C/min under nitrogen atmosphere. The crystallinity of PBS (X_{PBS}) was calculated based on the melting enthalpy of PBS (ΔH_{PBS}) occurring at ~112 °C and the weight ratio of PBS (W_{PBS}), as illustrated in eq 1.

$$X_{PBS} = \frac{\Delta H_{PBS}}{\Delta H^0_{PBS} \cdot W_{PBS}} \times 100\% \quad (1)$$

where ΔH^0_{PBS} represents the melting enthalpy of 100% crystalline PBS (220 J/g).[39] The crystallinity of PLA (X_{PLA}) based on the melting enthalpy near 173 °C was evaluated using the same method, while the melting enthalpy of 100% crystalline PLA is 93.7 J/g.[10]

Oxygen Permeability Measurements. The oxygen permeability (P_{O2}) of PLA/PBS composite films was determined at room temperature with 50% relative humidity and a VAC-V2 film permeability testing machine (labthink instruments, Jinan, China) according to ISO2556:1974. Oxygen gas (Alphagaz, Air Liquide Denmark) with a purity of >99.999% was used. Permeability coefficient of the composite films was calculated by an analysis program.[23] For each sample, measurements were repeated until four successive readings deviated <5% from the average value.

Mechanical Property Testing. According to ASTM standard D638:1999, the tensile properties were measured at room temperature on an Instron universal test instrument (Model 5576, Instron Instruments, USA) with a crosshead speed of 20 mm/min and a gauge length of 20 mm. A minimum of 6 bar for each sample was tested at the same conditions, and the average values were presented with standard deviation.

RESULTS AND DISCUSSION

Combining the in situ fibrillation and confined flaking techniques, we aim at creating and orderly organizing nanolaminar phase structure for PBS, potentially rendering the construction of compact "nano-barrier walls", as well as the generation of effective reinforcing elements.[40] Figure 2 offers the direct evidence of this. Figure 2a1 evidently suggests the formation of laminar PBS after confined flaking in the composite film penetrated 10 wt % PBS, in clear contrast to the nanofibrillated structure in the in situ fibrillar composite (Figure S2 of the Supporting Information). Figure 2a1,2 reveals some important features in the laminar structure of PBS. First, extremely high density and good alignment of PBS nanosheets are clearly observed, indicative of sufficient structural conversion from the rich, oriented PBS nanofibrils (Figure S2 of the Supporting Information). Second, these PBS nanosheets are characterized by a large width of 1.5 ± 0.3 μm but a low thickness of several to tens of nanometers, demonstrating little variations of volume compared to that of PBS nanofibrils with an average diameter of 83 nm. Such a high width/thickness ratio (428 ± 13.1 μm) of PBS nanosheets definitely may be on a par with or even exceed most 2D nanofillers such as nanoclay and few-layered graphene sheets.[23,25] Third, the PBS nanosheets are interconnected to each other to form an enormous laminar network without visible ends, primarily arising from the branched agglomeration of molten PBS nanofibrils during the confined flaking. The strong linkages created among the PBS nanosheets may present evident advantages over normal nanofillers that are individually dispersed in the matrix in terms of enhancing permeability resistance and mechanical performance.[30]

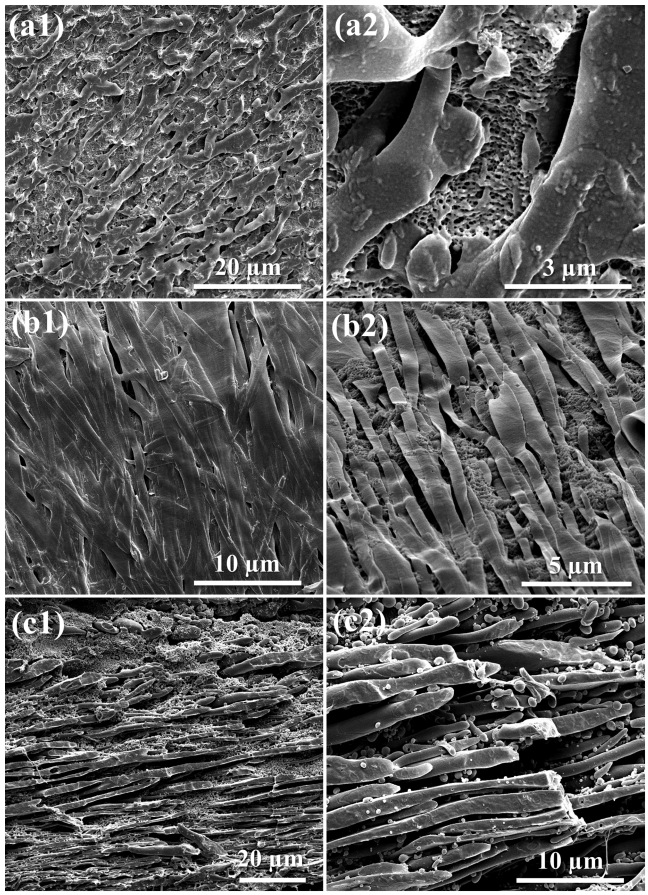

Figure 2. SEM images of section cryofracture surfaces of PLA/PBS composite films after etching the PLA matrix for (a1) PLA/PBS (90/10), (b1) PLA/PBS (80/20) and (c1) PLA/PBS (60/40); a2−c2 show the local morphology of PBS nanosheets in higher magnitude, respectively.

The significantly increased density of PBS nanosheets is clearly observed for the PLA/PBS (80/20) film in Figure 2b1,2, accompanied by the decreased width (0.9 ± 0.2 μm). The reduction in sheet width can be explained by the decreased viscosity of composite system in the presence of higher contents of PBS (Figure S3 of the Supporting Information), resulting in effective flow and extension of PBS fibrillar melts along the channels in PLA backbone. This restricts the lateral extension of PBS phase during the confined flaking, leading to the formation of orderly individual nanosheets rather than interconnected nanosheets in the PLA/PBS (90/10) film. Figure 2c1,2 suggests PBS nanofibrils in the PLA/PBS (60/40) sample cannot be effectively converted to nanosheets, displaying tabular ribbons with a width of 1.6 ± 0.3 μm are generated. The agglomeration of molten PBS phase and decreased channels of PLA framework are, to different degrees, responsible for it.

These observations evidently verify our first establishment of well-organized, thin and large PBS nanosheets in the PLA films, which has not been realized in the biomass-based system yet. Besides the desirable biocompatibility and degradability overwhelming traditional manufacture of polymeric nanocomposites, our proposed methodology offers some preponderant principles compared to the traditional manufacture of polymer "barrier walls" in polyolefins. It can be exemplified by the typical model based on polyethylene (matrix) and

DOI: 10.1021/acsami.5b00294
ACS Appl. Mater. Interfaces 2015, 7, 8023−8032

polyamide 6 (dispersed-phase).[41] The gross incompatibility of the immiscible blends is destined to cause asymmetrical distribution and dispersions of polyamide 6 and poor interfacial adhesion, frequently resulting in the low permeability resistance and easy breaking.[42] Incorporating a surfactant, compatibilizer or interfacial agent generally represents an indispensable route to prepare homogeneous blends prior to obtaining laminar polyamide 6.[32] In clear contrast, our case is established on the basis of common processing technology without utilizing any additives. Specifically, we have recently demonstrated that intensive shearing/stretching enabled the control of the structure and alignment of PBS, as well as the construction of ordered PLA lamellae at PBS nanofibrils which serve as tenacious filament to enhance the interfacial interactions.[36] The construction of aligned PBS nanofibrils, PLA lamellae and strong interfacial interactions satisfies essential prerequisites for creating oriented PBS nanosheets in the subsequent confined flaking process. Of more significance is the flexibility in the choice of biopolymer matrices based on this technique, probably motivating further efforts for creating laminar structure in biopolymer films.

Two-dimensional small-angle X-ray scattering (2D-SAXS) was performed to examine the ordered entities in PLA/PBS composite films (Figure 3). Figure 3A illustrates the 2D-SAXS patterns for the composite films, which yields the 1D intensity profiles, as plotted in Figure 3B. Only symmetrical bulb-shape lobes indicating the presence of oriented PLA lamellae are observed for the films containing 10 and 20 wt % PBS nanosheets, presumably due to the partial retention of oriented PLA units during the disengage of aligned PBS during confined flaking at 160 °C.[43] Moreover, the PLA/PBS (80/20) sample displays one more pair of lobes in the equatorial direction, probably arising from the orthogonal structure of woven PLA/PBS composites (Figure 1). Besides the existence of bulb-shape lobes, it is of great interest to observe a large scattering halo outside the lobes for the film incorporated 40 wt % PBS. It suggests the formation of a small quantity of less ordered PBS lamellae during the recrystallization in the confined space. Figure 3B manifests the PLA/PBS (90/10) and PLA/PBS (80/20) composite films present similar curves with a single peak at q = 0.12 and 0.14 nm^{-1}, respectively. The long period (L) corresponding to the intensity peak is calculated to be 52.3 and 44.8 nm for these two samples, respectively. Note that the L values of flaked composite films, which mainly reflects the lamellar spacing of PLA matrix, are twice over those of the as-stretched nanofibrillar composites (26.2 and 20.9 nm).[36] It primarily results from the synergetic morphological alterations of PLA matrix and dispersed PBS: (1) the creation of nanolaminar PBS during the confined flaking processing may interfere the ordered alignment of PLA lamellae in the vicinity of PBS nanosheets and thus expand the lamellar spacing; (2) the stretched PLA chains present high nucleation activity to form the lamellae with a higher thickness, which is likely facilitated by the neighboring PBS chains that are partially disengaged and relaxed (under 160 °C).[44,45] A broad and weak peak located at q = 0.44 nm^{-1} attributed to the PBS lamellae is exclusively observed for the film loaded 40 wt % PBS (Figure 3Bc), accompanied by the dominate peak at q = 0.15 nm^{-1}. Like the PLA matrix, the PBS lamellae (probably induced by the surviving stretched chains/segments) have a much higher long period of 14.3 nm compared to that of nanofibrils (8.4 nm).[36]

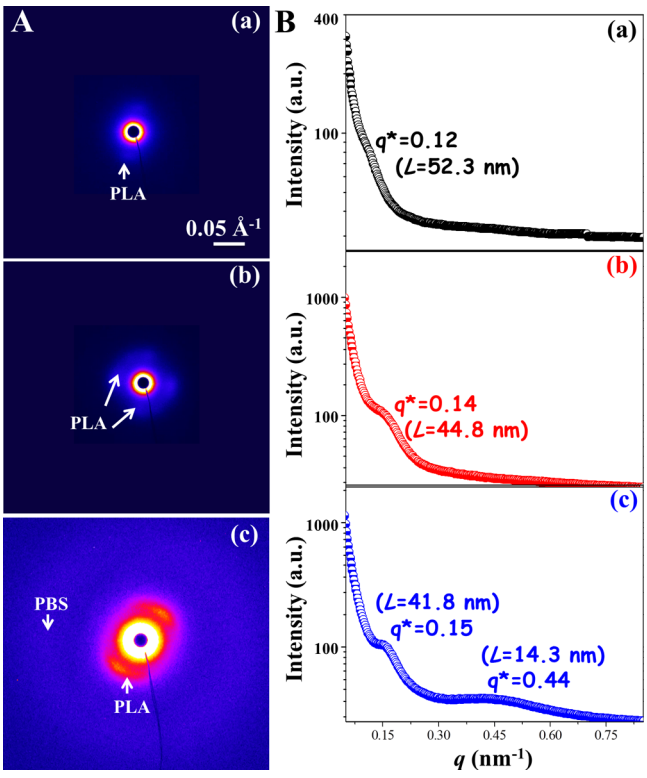

Figure 3. (A) Typical 2D-SAXS patterns and (B) 1D-SAXS intensity profiles of PLA/PBS composite films. Scattering patterns attributed to oriented PLA superstructures and epitaxial entities of PBS are indicated with white arrows in the 2D images. The peak position (q*) and long spacing (L) are marked near the peaks, and note that a broad and weak peak located at 0.44 nm^{-1} is observed as a result of epitaxial crystallization of PBS. (a) PLA/PBS (90/10), (b) PLA/PBS (80/20) and (c) PLA/PBS (60/40).

Crystalline morphology and molecular orientation of composite films are traced employing two-dimensional wide-angle X-ray scattering (2D-WAXD), as presented in Figure 4. Arc-like diffraction patterns assigned to oriented lattice planes (010), (200)/(100) and (203) of α-form PLA are observed for both PLA/PBS (90/10) and PLA/PBS (80/20) in Figure 4A, giving rise to the main diffraction reflection at 2θ = 15.8°, 16.7° and 18.9° for PLA, respectively (Figure 4B).[46,47] Homogeneous diffraction rings with strong intensity are detected for PLA in the film incorporated 40 wt % PBS (Figure 4A), displaying weak PBS reflection close to the lattice planes of PLA (Figure 4B). It is evident that the 2D-WAXD characterization yields the same results with the 2D-SAXS analysis, i.e., the retention of oriented PLA units enables the generation of ordered PLA lamellae for films containing 10 and 20 wt % PBS nanosheets in the confined flaking process. This assumption explains, in principle, the high orientation degree of PLA for the two samples, but substantially decreased orientation parameter for the film after incorporating 40 wt % PBS (Figure 4C).

Differential scanning calorimetry (DSC) was carried out to offer insights into the thermal behaviors of composite films in the presence of PBS nanosheets, as recorded in Figure 5. Pure PLA film submitted to the same processing was also measured to distinguish the thermal transitions from those of PBS (Figure 5a). Figure 5a clearly indicates pure PLA displays a glass transition at 59.9 °C (T_g) and a melting endotherm at 172.9 °C, and the crystallinity (46.6%) is found to be much higher than that of as-stretched pure PLA (11.4%).[36] It is well in line

DOI: 10.1021/acsami.5b00294
ACS Appl. Mater. Interfaces 2015, 7, 8023−8032

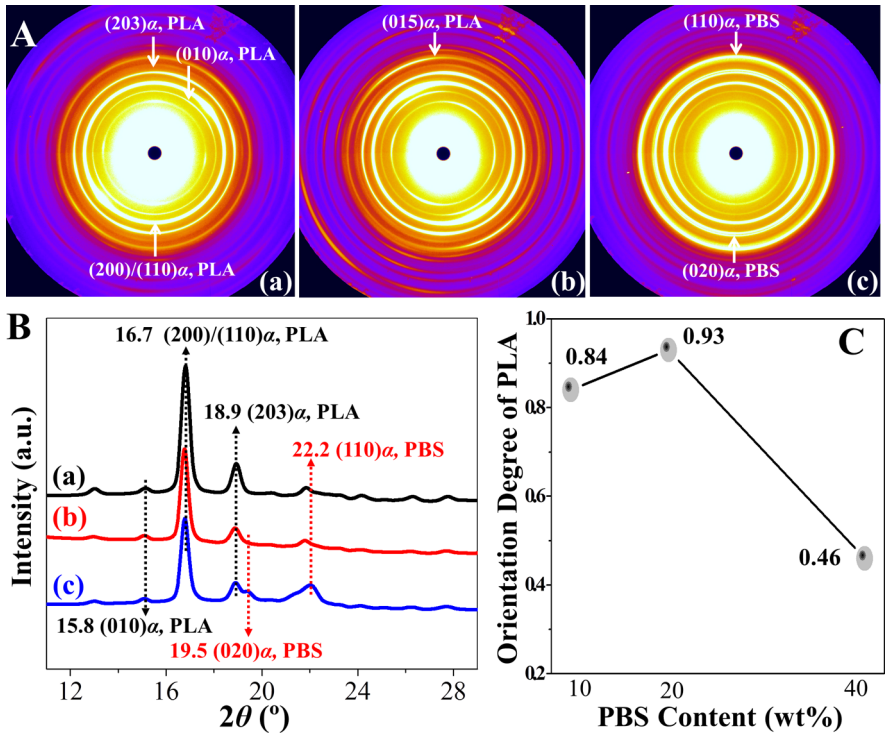

Figure 4. (A) Representative 2D-WAXD patterns and (B) 1D-WAXD intensity profiles of PLA/PBS composite films, the diffraction peaks and their assignment to the specific lattice planes are indicated on the curves (black dashed lines for the diffraction peaks of PLA and red ones for PBS). (C) Plots of orientation degree of PLA as a function of PBS content. The orientation parameter is calculated based on the azimuth angle (0–360°) of lattice plane (200)/(110) due to its highest diffraction intensity in all reflections of PLA. (a) PLA/PBS (90/10), (b) PLA/PBS (80/20) and (c) PLA/PBS (60/40).

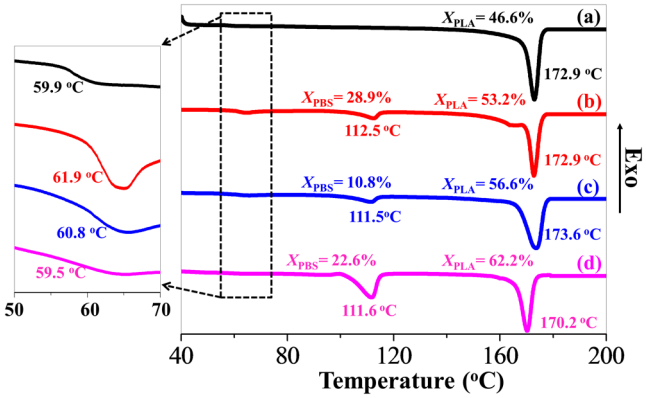

Figure 5. Heating traces of the DSC program of (a) pure PLA, (b) PLA/PBS (90/10), (c) PLA/PBS (80/20) and (d) PLA/PBS (60/40) composite films. The glass transition temperature (T_g) and the melting points of PBS and PLA (T_{m1}, T_{m2}) are marked below the curves. Crystallinity of PBS and PLA (X_{PBS}, X_{PLA}) marked on the curves is calculated on the basis of their melting enthalpies and weight ratios, respectively. The glass transition region is extracted to present clear identification of T_g shifts. The curves in the range of 30–40 °C were disordered and not plotted due to the overshoot of heat flow at the beginning of the thermoprogram.

with the SAXS results and again confirms our hypothesis on the reorganization of ordered lamellae staring from the aligned PLA chains. With the incorporation of PBS nanosheets, some notable variations of thermal behaviors are observed. First, T_g of PLA jumps to 61.9 °C for PLA/PBS (90/10) and decreases to 60.8 and 59.5 °C for the films containing 20 and 40 wt % PBS. It mainly results from the competition between the formation of interlinked or individual nanosheets strongly interacting with the PLA chains that pushes up the T_g values and the introduction of flexible PBS chains that causes the reduction of T_g.[46,48] Second, small endotherm peaks ascribed to the melting of PBS are located at ~112 °C. One may notice that the PLA/PBS (90/10) film presents the highest melting point at 112.5 °C, which is principally associated with the existence of interconnected PBS networks that immobilize the adjacent PLA chains. Third, the crystallinity of PLA ranges from 53.2 to 62.2%, well above that of PBS (normally lower than 30%). This provides sufficient evidence for extended PLA chains in serving as the precursors to elicit the rapid generation of ordered lamellae.[49] Additionally, PLA/PBS (60/40) shows the lowest melting point of PLA at 170.2 °C, mainly due to the increase of PBS chains with high mobility and low melting point.

The above observations confirm the establishment of PBS phase displaying distinct structural features: enormous nanosheets interconnected to each other for PLA/PBS (90/10), individual nanosheets with a higher concentration and tabular ribbons in the films penetrated 20 and 40 wt % PBS. The existence of these nanolaminar blocks lays down important prerequisites for the enhancement of barrier ability. Figure 6A reveals the large changes in oxygen permeability coefficient (P_{O2}) for the composite films. Evidently, the highest permeability (1.4×10^{-14} $cm^3 \cdot cm \cdot cm^{-2} \cdot s^{-1} \cdot Pa^{-1}$) occurs in pure PLA film, and pure PBS film shows a much lower P_{O2} at 0.6×10^{-14} $cm^3 \cdot cm \cdot cm^{-2} \cdot s^{-1} \cdot Pa^{-1}$. It is a surprise to find the substantial decrease in P_{O2} for all composite films (even lower than that of pure PBS). In particular, PLA/PBS (80/20) is characterized by the lowest P_{O2} of 0.2×10^{-14} $cm^3 \cdot cm \cdot cm^{-2} \cdot s^{-1} \cdot Pa^{-1}$, whereas moderately increased P_{O2} values are observed

DOI: 10.1021/acsami.5b00294
ACS Appl. Mater. Interfaces 2015, 7, 8023–8032

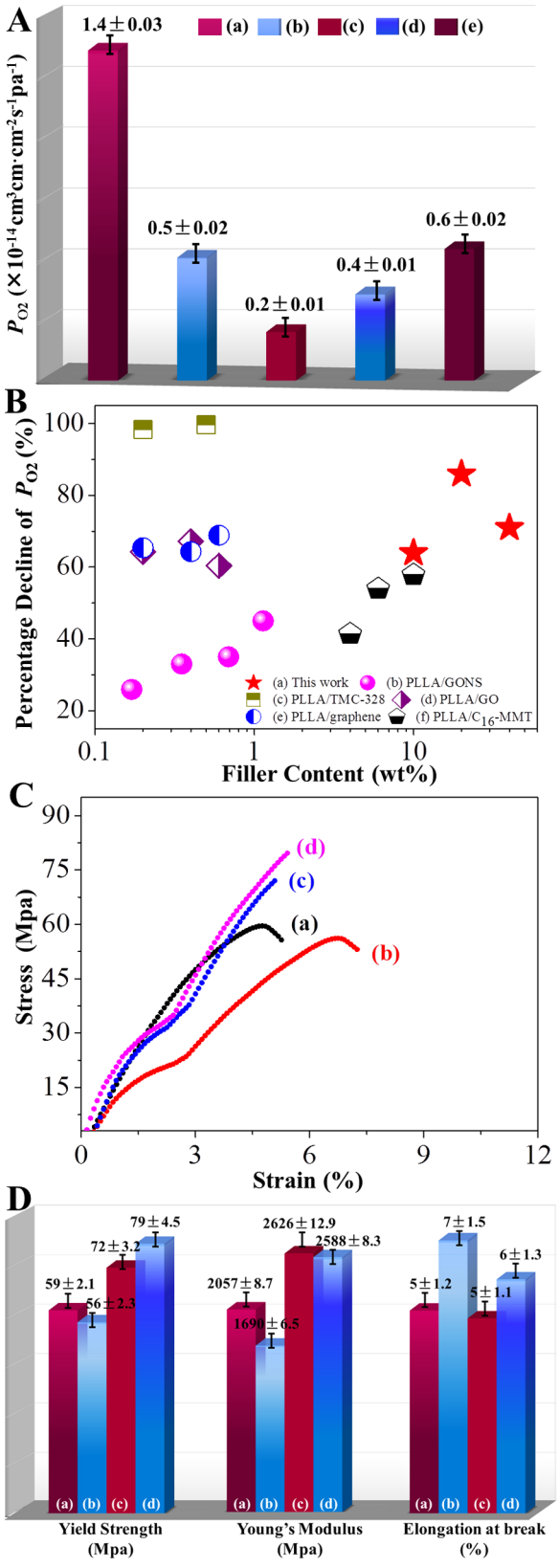

Figure 6. Performance evaluation to demonstrate the impressive permeability resistance to oxygen of the PLA films containing PBS nanosheets, as well as the exceptional mechanical properties. (A) Bar chart showing the values of oxygen permeability coefficient (P_{O2}) with standard deviations for (a) pure PLA, (b) PLA/PBS (90/10), (c) PLA/PBS (80/20), (d) PLA/PBS (60/40) and (e) pure PBS. (B) Comparison of percentage decline of P_{O2} between (a) this work and other PLLA composite systems based on (b) GO nanosheets,[23] (c) *N*,*N*′,*N*″-Tricyclohexyl-1,3,5-benzenetricarboxylamide (trade name TMC-328, a nucleating agent of PLLA),[18] (d) GO,[24] (e) graphene[24] and (f) hexadecylamine−montmorillonite (C16-MMT),[67] the percentage decline is defined as the decrease in P_{O2} to the initial value of pure matrix. (C) Typical strain−stress curves and (D) detailed tensile results regarding yield strength, Young's modulus, elongation at break for (a) pure PLA, (b) PLA/PBS (90/10), (c) PLA/PBS (80/20) and (d) PLA/PBS (60/40).

for composite films with 20 and 40 wt % PBS (0.5 and 0.4 × 10^{-14} cm^3·cm·cm^{-2}·s^{-1}·Pa^{-1}). Apparently, the barrier properties of composite films are closely associated with the phase morphology of incorporated PBS. For PLA/PBS (80/20) composite film, an array of compact, well-organized PBS nanosheets render the construction of robust barriers to the diffusing gas molecules, conferring the highest promotion in the permeability resistance.[50] This mechanism can be further enhanced by the increased concentration of crystalline phase of PLA due to the enhancement of crystallization kinetics with the aid of the existing PBS nanosheets (Figures 4 and 5), forcing a tortuous penetration path for the gas molecules by offering compact crystalline lamellae.[18,51,52] As such, the PLA/PBS (60/40) shows moderately higher permeability in the absence of sufficiently flaked PBS nanosheets, suggesting that 1D structural units (or fillers) fail to provide effective resistance to gas diffusion and permeation compared to the 2D ones. It is therefore instructive to convert 1D structural units into 2D ones to advance barrier properties, instead of traditional preparation of nanocomposites based on nanotubes and nanowhiskers.[53−57] Although unique interconnected nanosheets are created for PLA/PBS (90/10), the low concentration of "barrier walls" slightly pushes up the oxygen permeability. It should be emphasized that PLA/PBS blends manufactured by common processing methods are normally characterized by poor barrier performance, instead of translating the relatively high barrier ability of PBS to the PLA products. As an example, Gupta et al. demonstrated the PLA/PBS blends loaded 20 wt % PBS prepared by extrusion compounding followed by confined flaking presented almost the same oxygen permeability with pure PLA (around 20 cm^3·mm·m^{-2}·day^{-1}·atm).[58] It seems that uncontrollable phase morphology and poor phase interface in the immiscible blends cause the easy diffusion and permeation of gas molecules through the PLA matrix and interfaces.[44,59] Figure 6B clarifies the distinct superiority of our proposed methodology, i.e., tailoring the phase morphology holds the potential to achieve superior oxygen-barrier properties in fully biodegradable composites film.

Next, we examined the enormous possibility of developing PBS nanosheets in largely improving the mechanical properties of PLA, as indicated in Figure 6C,D. We see from Figure 6C that the composite films present similar tensile behavior with pure PLA, starting from elastic deformation and fracturing with slight plastic deformation. Some important parameters of the tensile properties are summarized in Figure 6D. Of particular significance is the proportional relationship between the strength and stiffness of composite films and the content of oriented PBS units. Compared to the value of 59.5 MPa for pure PLA, the incorporation of PBS is found to give an unusual enhancement of yield strength up to 72.1 and 79.1 MPa for PLA/PBS (80/20) and PLA/PBS (60/40), respectively. Note

DOI: 10.1021/acsami.5b00294
ACS Appl. Mater. Interfaces 2015, 7, 8023−8032

that pure PBS film intrinsically shows low tensile strength and modulus of 33.7 and 623 MPa, respectively, well below those of pure PLA (Figure S5 of the Supporting Information). The highly ordered PBS nanosheets can serve as the effective reinforcing elements instead producing the simple plasticization for the common PLA/PBS blends.[48,60] This is the reason for the slightly decreased strength observed in PLA/PBS (90/10) film containing the lowest content of PBS nanosheets (56.1 MPa). Similar results are found in the Young's modulus of composite films, achieving the profoundly increased modulus for PLA/PBS (80/20) and PLA/PBS (60/40) (2626 and 2588 MPa) in comparison to low modulus of pure PLA (2057 MPa). Moreover, PLA/PBS (90/10) presents the highest elongation at break (7.1%), which can be appraised from the formation of interconnected nanosheets that may show strong retardation of crack propagation with the dissipation and absorption of much energy when encountering the stress deformation.

The unusual combination of barrier properties and mechanical performances suggests appealing generalizations concerning the role of laminar structuring in encouraging evolutionary innovations and adaptive radiation for achieving high performance and functionalities for PLA. Practically, the traditional blend or composite systems such as PLA/PBS and PLA/graphene associated with the normal processing technique (e.g., solution casting, extrusion, compression, injection molding, and spinning) have unfortunately resulted in undesirable balance of permeability resistance and mechanical properties.[61] Limited progress in simultaneous enhancement of barrier and mechanical properties was found in the PLA composites and blends, even in the recent reports.[62−65] Here the polymeric nanosheets with enormous specific surface area are providing their extremes to resist gas permeation and stress deformation, which is essentially attractive both academically and commercially.[66]

In addition to the distinct superiority in offering high resistance to oxygen permeation compared to the traditional PLA-based composing systems, our PLA/PBS composite films featuring the combination of high mechanical properties and low gas permeation can even challenge the common plastic films existing in the market, as illustrated in Figure 7. Although making up a huge share of the films market, polyethylene (PE), polypropylene (PP), polystyrene (PS) and poly(vinyl chloride) (PVC) are characterized by the relatively poor barrier properties compared to our PLA/PBS composite films, by for example showing a P_{O2} of 5−10 × 10^{-14} $cm^3 \cdot cm \cdot cm^{-2} \cdot s^{-1} \cdot Pa^{-1}$ for PP films.[68] More importantly, these traditional films normally fall into the category of poor mechanical properties, as demonstrated by the tensile strength of 50−60 MPa for PVC films—far below that of our PLA/PBS films (up to nearly 80 MPa). It is apparent that our PLA/PBS composite films are in the comparable level with poly(ethylene terephthalate) (PET) with respect to the ability to resist gas molecules diffusion, both of which present the extremely low values of P_{O2} (0.1−0.6 × 10^{-14} $cm^3 \cdot cm \cdot cm^{-2} \cdot s^{-1} \cdot Pa^{-1}$).[68] The property elucidation evidently brings to light the possibility to substitute the fossil-fuel films with biobased materials. As growing industrial development drastically reduces the production costs of bioplastics, scaled-up biorefineries can ultimately compete with those traditional plastics coming only from crude oil.[69]

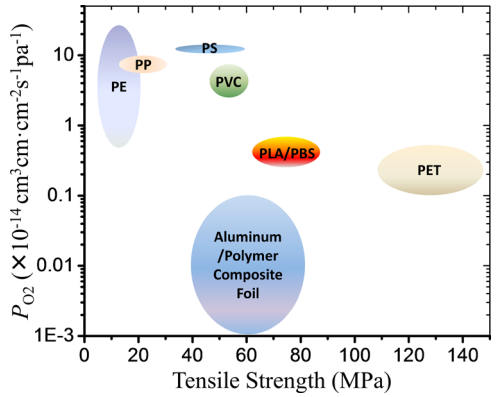

Figure 7. Comparison of P_{O2} and tensile strength for a wide range of packaging film materials, showing that our PLA films containing nanolaminar PBS present the distinct combination of low P_{O2} and high strength even compared to the common packaging materials existing in the films market. Although the aluminum/polymer (e.g., PP or PET) composite foils frequently used as food containers stand out in the comparison of barrier properties, people can expect the growing urgency to pursue sustainable developments and substitute these packaging materials with the renewable and degradable candidates, such as our PLA/PBS composite films. A factor of 0.1143 × 10^{-14} was used to transfer the data of P_{O2} reported from the literature[68] to allow the direct comparison with our work, i.e., 1 $cm^3 \cdot mm \cdot m^{-2} \cdot day^{-1} \cdot atm^{-1}$ = 0.1143 × 10^{-14} $cm^3 \cdot cm \cdot cm^{-2} \cdot s^{-1} \cdot Pa^{-1}$.

CONCLUSIONS

In the present work, fully biodegradable PLA films incorporated PBS nanosheets were achieved by converting PBS nanofibrils into nanosheets during a simple confined flaking at 160 °C. The specific molding temperature allowed for the sufficient thermal deformation of PBS nanofibrils and retention of ordered PLA channels. Large, well-ordered PBS nanosheets with a thickness of several to tens of nanometers were observed in the composite films loaded 10 and 20 wt % PBS, whereas PLA/PBS (60/40) only showed tabular ribbons primarily due to insufficient lateral deformation with high PBS content. Resulting from an array of compact aligned PBS nanosheets serving as robust "barrier walls", drastically improved resistance to oxygen was observed for all composite films, and the highest decrease of 86% and 67% in oxygen permeability coefficient was achieved for the PLA/PBS (80/20) film compared to pure PLA (1.4 × 10^{-14} $cm^3 \cdot cm \cdot cm^{-2} \cdot s^{-1} \cdot Pa^{-1}$) and pure PBS (0.6 × 10^{-14} $cm^3 \cdot cm \cdot cm^{-2} \cdot s^{-1} \cdot Pa^{-1}$), respectively. Unexpectedly, the tensile strength and stiffness of composite films increased gradually with the introduction of extended PBS. It can be exemplified by the rise of strength and modulus up to 72.1 and 2626 MPa for the composite film loaded 20 wt %, showing a prominent increase of 21% and 28% compared to pure PLA. The unusual combination of barrier and mechanical performances of PLA films penetrated nanolaminar PBS represents specific properties required for green packaging beverage. More importantly, our tentative exploration of high-performance and functional PLA films based on confined flaking signifies potential in its broad application to the industrially feasible manufacturing such as successive rolling. Looking out to the future, with the growing number of preparation, structuring and engineering pathways to specific phase architectures and nanostructured sheets in the materials scientists' hands, it appears likely to increasingly structure tailor-made creation of sheet-like biopolymer "nano-barrier walls".

DOI: 10.1021/acsami.5b00294
ACS Appl. Mater. Interfaces 2015, 7, 8023−8032

■ ASSOCIATED CONTENT

Supporting Information

Schematic representation of the "slit die extrusion-hot stretching-quenching" technique, SEM observation of phase morphology of PLA/PBS blends after extrusion compounding and PLA/PBS nanofibrillar composites after hot stretching, frequency dependency of complex viscocity (η) of PLA/PBS blends, and DSC heating trace and tensile properties of pure PBS film. This material is available free of charge via the Internet at http://pubs.acs.org.

■ AUTHOR INFORMATION

Corresponding Authors

*Z.-M. Li. Email: zmli@scu.edu.cn.

*G.-J. Zhong. Email: ganji.zhong@scu.edu.cn.

Notes

The authors declare no competing financial interest.

■ ACKNOWLEDGMENTS

The authors are deeply indebted to Yan-Hui Chen, Xu-Juan Li, Dong Zhou and Hua-Dong Huang for their kind help in performing SAXS, WAXD and oxygen permeability measurements. This work is financially supported by the China Scholarship Council (CSC), the National Natural Science Foundation of China (Grants 51120135002, 21276168, 51473101 and 51421061), the Innovation Team Program of Science & Technology Department of Sichuan Province (Grant 2014TD0002) and the Doctoral Program of the Ministry of Education of China (Grant 20130181130012).

■ REFERENCES

(1) Wang, H.; Xu, M.; Wu, Z.; Zhang, W.; Ji, J.; Chu, P. K. Biodegradable Poly(butylene succinate) Modified by Gas Plasmas and Their in Vitro Functions as Bone Implants. *ACS Appl. Mater. Interfaces* **2012**, *4*, 4380−4386.

(2) Venkataraman, P.; Tang, J.; Frenkel, E.; McPherson, G. L.; He, J.; Raghavan, S. R.; Kolesnichenko, V.; Bose, A.; John, V. T. Attachment of a Hydrophobically Modified Biopolymer at the Oil−Water Interface in the Treatment of Oil Spills. *ACS Appl. Mater. Interfaces* **2013**, *5*, 3572−3580.

(3) Svagan, A. J.; Berglund, L. A.; Jensen, P. Cellulose Nanocomposite Biopolymer Foam—Hierarchical Structure Effects on Energy Absorption. *ACS Appl. Mater. Interfaces* **2011**, *3*, 1411−1417.

(4) Shi, Y.; Jiang, S.; Zhou, K.; Bao, C.; Yu, B.; Qian, X.; Wang, B.; Hong, N.; Wen, P.; Gui, Z.; Hu, Y.; Yuen, R. K. K. Influence of g-C3N4 Nanosheets on Thermal Stability and Mechanical Properties of Biopolymer Electrolyte Nanocomposite Films: A Novel Investigation. *ACS Appl. Mater. Interfaces* **2013**, *6*, 429−437.

(5) Zhao, W.; Glavas, L.; Odelius, K.; Edlund, U.; Albertsson, A. C. Facile and Green Approach towards Electrically Conductive Hemicellulose Hydrogels with Tunable Conductivity and Swelling Behavior. *Chem. Mater.* **2014**, *26*, 4265−4273.

(6) Martins, A. M.; Eng, G.; Caridade, S. G.; Mano, J. F.; Reis, R. L.; Vunjak-Novakovic, G. Electrically Conductive Chitosan/Carbon Scaffolds for Cardiac Tissue Engineering. *Biomacromolecules* **2014**, *15*, 635−643.

(7) Thayer, P. S.; Dimling, A. F.; Plessl, D. S.; Hahn, M. R.; Guelcher, S. A.; Dahlgren, L. A.; Goldstein, A. S. Cellularized Cylindrical Fiber/Hydrogel Composites for Ligament Tissue Engineering. *Biomacromolecules* **2013**, *15*, 75−83.

(8) Li, J. J.; Gil, E. S.; Hayden, R. S.; Li, C.; Roohani-Esfahani, S. I.; Kaplan, D. L.; Zreiqat, H. Multiple Silk Coatings on Biphasic Calcium Phosphate Scaffolds: Effect on Physical and Mechanical Properties and In Vitro Osteogenic Response of Human Mesenchymal Stem Cells. *Biomacromolecules* **2013**, *14*, 2179−2188.

(9) Xie, L.; Xu, H.; Wang, Z.-P.; Li, X. J.; Chen, J. B.; Zhang, Z. J.; Yin, H. M.; Zhong, G. J.; Lei, J.; Li, Z. M. Toward Faster Degradation for Natural Fiber Reinforced Poly(lactic acid) Biocomposites by Enhancing the Hydrolysis-Induced Surface Erosion. *J. Polym. Res.* **2014**, *21*, 357−371.

(10) Xu, H.; Liu, C. Y.; Chen, C.; Hsiao, B. S.; Zhong, G. J.; Li, Z. M. Easy Alignment and Effective Nucleation Activity of Ramie Fibers in Injection-Molded Poly(lactic acid) Biocomposites. *Biopolymers* **2012**, *97*, 825−839.

(11) Inkinen, S.; Hakkarainen, M.; Albertsson, A. C.; Södergård, A. From Lactic Acid to Poly(lactic acid) (PLA): Characterization and Analysis of PLA and Its Precursors. *Biomacromolecules* **2011**, *12*, 523−532.

(12) Zhang, K.; Nagarajan, V.; Misra, M.; Mohanty, A. K. Supertoughened Renewable PLA Reactive Multiphase Blends System: Phase Morphology and Performance. *ACS Appl. Mater. Interfaces* **2014**, *6*, 12436−12448.

(13) Wang, T.; Drzal, L. T. Cellulose-Nanofiber-Reinforced Poly(lactic acid) Composites Prepared by a Water-based Approach. *ACS Appl. Mater. Interfaces* **2012**, *4*, 5079−5085.

(14) Arias, V.; Höglund, A.; Odelius, K.; Albertsson, A. C. Tuning the Degradation Profiles of Poly(L-lactide)-based Materials through Miscibility. *Biomacromolecules* **2013**, *15*, 391−402.

(15) Xu, H.; Xie, L.; Jiang, X.; Li, X. J.; Li, Y.; Zhang, Z. J.; Zhong, G. J.; Li, Z. M. Toward Stronger Transcrystalline Layers in Poly(L-lactic acid)/Natural Fiber Biocomposites with the Aid of an Accelerator of Chain Mobility. *J. Phys. Chem. B* **2014**, *118*, 812−823.

(16) Hu, Y.; Gu, X.; Yang, Y.; Huang, J.; Hu, M.; Chen, W.; Tong, Z.; Wang, C. Facile Fabrication of Poly(L-lactic acid)-Grafted Hydroxyapatite/Poly(lactic-co-glycolic acid) Scaffolds by Pickering High Internal Phase Emulsion Templates. *ACS Appl. Mater. Interfaces* **2014**, *6*, 17166−17175.

(17) Li, D.; Sun, H.; Jiang, L.; Zhang, K.; Liu, W.; Zhu, Y.; Fangteng, J.; Shi, C.; Zhao, L.; Sun, H.; Yang, B. Enhanced Biocompatibility of PLGA Nanofibers with Gelatin/Nano-Hydroxyapatite Bone Biomimetics Incorporation. *ACS Appl. Mater. Interfaces* **2014**, *6*, 9402−9410.

(18) Bai, H.; Huang, C.; Xiu, H.; Zhang, Q.; Deng, H.; Wang, K.; Chen, F.; Fu, Q. Significantly Improving Oxygen Barrier Properties of Polylactide via Constructing Parallel-Aligned Shish-Kebab-Like Crystals with Well-Interlocked Boundaries. *Biomacromolecules* **2014**, *15*, 1507−1514.

(19) Delpouve, N.; Stoclet, G.; Saiter, A.; Dargent, E.; Marais, S. Water Barrier Properties in Biaxially Drawn Poly(lactic acid) Films. *J. Phys. Chem. B* **2012**, *116*, 4615−4625.

(20) Mattioli, S.; Peltzer, M.; Fortunati, E.; Armentano, I.; Jiménez, A.; Kenny, J. M. Structure, Gas-Barrier Properties and Overall Migration of Poly(lactic acid) Films Coated with Hydrogenated Amorphous Carbon Layers. *Carbon* **2013**, *63*, 274−282.

(21) Aulin, C.; Karabulut, E.; Tran, A.; Wågberg, L.; Lindström, T. Transparent Nanocellulosic Multilayer Thin Films on Polylactic Acid with Tunable Gas Barrier Properties. *ACS Appl. Mater. Interfaces* **2013**, *5*, 7352−7359.

(22) Chang, J.-H.; An, Y. U.; Sur, G. S. Poly(lactic acid) Nanocomposites with Various Organoclays. I. Thermomechanical Properties, Morphology, and Gas Permeability. *J. Polym. Sci., Part B: Polym. Phys.* **2003**, *41*, 94−103.

(23) Huang, H. D.; Ren, P. G.; Xu, J. Z.; Xu, L.; Zhong, G. J.; Hsiao, B. S.; Li, Z. M. Improved Barrier Properties of Poly(lactic acid) with Randomly Dispersed Graphene Oxide Nanosheets. *J. Membr. Sci.* **2014**, *464*, 110−118.

(24) Pinto, A. M.; Cabral, J.; Tanaka, D. A. P.; Mendes, A. M.; Magalhães, F. D. Effect of Incorporation of Graphene Oxide and Graphene Nanoplatelets on Mechanical and Gas Permeability Properties of Poly(lactic acid) Films. *Polym. Int.* **2013**, *62*, 33−40.

(25) Carosio, F.; Colonna, S.; Fina, A.; Rydzek, G.; Hemmerlé, J.; Jierry, L.; Schaaf, P. Efficient Gas and Water Vapor Barrier Properties of Thin Poly(lactic acid) Packaging Films: Functionalization with Moisture Resistant Nafion and Clay Multilayers. *Chem. Mater.* **2014**, *26*, 5459−5466.

DOI: 10.1021/acsami.5b00294
ACS Appl. Mater. Interfaces 2015, 7, 8023−8032

(26) Guo, F.; Silverberg, G.; Bowers, S.; Kim, S. P.; Datta, D.; Shenoy, V.; Hurt, R. H. Graphene-based Environmental Barriers. *Environ. Sci. Technol.* **2012**, *46*, 7717−7724.
(27) Compton, O. C.; Kim, S.; Pierre, C.; Torkelson, J. M.; Nguyen, S. T. Crumpled Graphene Nanosheets as Highly Effective Barrier Property Enhancers. *Adv. Mater.* **2010**, *22*, 4759−4763.
(28) Creighton, M. A.; Ohata, Y.; Miyawaki, J.; Bose, A.; Hurt, R. H. Two-Dimensional Materials as Emulsion Stabilizers: Interfacial Thermodynamics and Molecular Barrier Properties. *Langmuir* **2014**, *30*, 3687−3696.
(29) Fakirov, S.; Evstatiev, M.; Petrovich, S. Microfibrillar Reinforced Composites from Binary and Ternary Blends of Polyesters and Nylon 6. *Macromolecules* **1993**, *26*, 5219−5226.
(30) Wu, Q.; Xu, Y.; Yao, Z.; Liu, A.; Shi, G. Supercapacitors Based on Flexible Graphene/Polyaniline Nanofiber Composite Films. *ACS Nano* **2010**, *4*, 1963−1970.
(31) Cao, Y.; Feng, J.; Wu, P. Preparation of Organically Dispersible Graphene Nanosheet Powders through a Lyophilization Method and Their Poly(lactic acid) Composites. *Carbon* **2010**, *48*, 3834−3839.
(32) Subramanian, P. Permeability Barriers by Controlled Morphology of Polymer Blends. *Polym. Eng. Sci.* **1985**, *2*, 483−487.
(33) Subramanian, P. M.; Mehra, V. Laminar Morphology in Polymer Blends: Structure and Properties. *Polym. Eng. Sci.* **1987**, *27*, 663−668.
(34) Yeh, J. T.; Jyan, C. F. Effects of Polyethylenes on the Morphology, Barrier, and Impact Properties of Polyethylene/Modified Polyamide Blends. *Polym. Eng. Sci.* **1998**, *38*, 1482−1490.
(35) Yeh, J. T.; Shih, W. H.; Huang, S. S. Paint Solvent Permeation Resistance of Polyethylene, Polyethylene/Polyamide and Polyethylene/Modified Polyamide Bottles. *Macromol. Mater. Eng.* **2002**, *287*, 23−30.
(36) Xie, L.; Xu, H.; Niu, B.; Ji, X.; Chen, J.; Li, Z. M.; Hsiao, B. S.; Zhong, G. J. Unprecedented Access to Strong and Ductile Poly(lactic acid) by Introducing In Situ Nanofibrillar Poly(butylene succinate) for Green Packaging. *Biomacromolecules* **2014**, *15*, 4054−4064.
(37) Evstatiev, M.; Fakirov, S.; Bechtold, G.; Friedrich, K. Structure-Property Relationships of Injection- and Compression-Molded Microfibrillar-Reinforced PET/PA-6 Composites. *Adv. Polym. Technol.* **2000**, *19*, 249−259.
(38) Picken, S. J.; Aerts, J.; Visser, R.; Northolt, M. G. Structure and Rheology of Aramid Solutions: X-ray Scattering Measurements. *Macromolecules* **1990**, *23*, 3849−3854.
(39) Signori, F.; Pelagaggi, M.; Bronco, S.; Righetti, M. C. Amorphous/Crystal and Polymer/Filler Interphases in Biocomposites from Poly(butylene succinate). *Thermochim. Acta* **2012**, *543*, 74−81.
(40) Fakirov, S. Nano-/Microfibrillar Polymer−Polymer and Single Polymer Composites: The Converting Instead of Adding Concept. *Compos. Sci. Technol.* **2013**, *89*, 211−225.
(41) Yeh, J. T.; Fan-Chiang, C. C.; Cho, M. F. Effects of Compatibilizer Precursors on the Barrier Properties and Morphology of Polyethylene/Polyamide Blends. *Polym. Bull.* **1995**, *35*, 371−378.
(42) Yeh, J.-T.; Fan-Chiang, C.-C. Permeation Mechanisms of Xylene in Blow-Molded Bottles of Pure Polyethylene, Polyethylene/Polyamide and Polyethylene/Modified Polyamide Blends. *J. Polym. Res.* **1996**, *3*, 211−219.
(43) Xu, H.; Xie, L.; Chen, J. B.; Jiang, X.; Hsiao, B. S.; Zhong, G. J.; Fu, Q.; Li, Z. M. Strong and Tough Micro/Nanostructured Poly(lactic acid) by Mimicking Multifunctional Hierarchy of Shell. *Mater. Horiz.* **2014**, *1*, 546−552.
(44) Wu, D.; Yuan, L.; Laredo, E.; Zhang, M.; Zhou, W. Interfacial Properties, Viscoelasticity, and Thermal Behaviors of Poly(butylene succinate)/Polylactide Blend. *Ind. Eng. Chem. Res.* **2012**, *51*, 2290−2298.
(45) Ojijo, V.; Ray, S. S.; Sadiku, R. Toughening of Biodegradable Polylactide/Poly(butylene succinate-co-adipate) Blends via in Situ Reactive Compatibilization. *ACS Appl. Mater. Interfaces* **2013**, *5*, 4266−4276.
(46) Xu, H.; Zhong, G. J.; Fu, Q.; Lei, J.; Jiang, W.; Hsiao, B. S.; Li, Z. M. Formation of Shish-Kebabs in Injection-Molded Poly(L-lactic acid) by Application of an Intense Flow Field. *ACS Appl. Mater. Interfaces* **2012**, *4*, 6774−6784.
(47) Xu, H.; Xie, L.; Jiang, X.; Hakkarainen, M.; Chen, J. B.; Zhong, G. J.; Li, Z. M. Structural Basis for Unique Hierarchical Cylindrites Induced by Ultrahigh Shear Gradient in Single Natural Fiber Reinforced Poly(lactic acid) Green Composites. *Biomacromolecules* **2014**, *15*, 1676−1686.
(48) Zhang, K.; Mohanty, A. K.; Misra, M. Fully Biodegradable and Biorenewable Ternary Blends from Polylactide, Poly(3-hydroxybutyrate-co-hydroxyvalerate) and Poly(butylene succinate) with Balanced Properties. *ACS Appl. Mater. Interfaces* **2012**, *4*, 3091−3101.
(49) Xu, H.; Xie, L.; Chen, Y. H.; Huang, H. D.; Xu, J. Z.; Zhong, G. J.; Hsiao, B. S.; Li, Z. M. Strong Shear Flow-Driven Simultaneous Formation of Classic Shish-Kebab, Hybrid Shish-Kebab and Transcrystallinity in Poly(lactic acid)/Natural Fiber Biocomposites. *ACS Sustainable Chem. Eng.* **2013**, *1*, 1619−1629.
(50) Kim, H.; Miura, Y.; Macosko, C. W. Graphene/Polyurethane Nanocomposites for Improved Gas Barrier and Electrical Conductivity. *Chem. Mater.* **2010**, *22*, 3441−3450.
(51) Drieskens, M.; Peeters, R.; Mullens, J.; Franco, D.; Lemstra, P. J.; Hristova-Bogaerds, D. G. Structure Versus Properties Relationship of Poly(lactic acid). I. Effect of Crystallinity on Barrier Properties. *J. Polym. Sci., Part B: Polym. Phys.* **2009**, *47*, 2247−2258.
(52) Evstatiev, M.; Simeonova, S.; Friedrich, K.; Pei, X.-Q.; Formanek, P. MFC-Structured Biodegradable Poly(L-lactide)/Poly(butylene adipate-*co*-terephatalate) Blends with Improved Mechanical and Barrier Properties. *J. Mater. Sci.* **2013**, *48*, 6312−6330.
(53) Thielemans, W.; Warbey, C. R.; Walsh, D. A. Permselective Nanostructured Membranes Based on Cellulose Nanowhiskers. *Green Chem.* **2009**, *11*, 531−537.
(54) Sánchez-García, M. D.; Hilliou, L.; Lagarón, J. M. Morphology and Water Barrier Properties of Nanobiocomposites of κ/ι-Hybrid Carrageenan and Cellulose Nanowhiskers. *J. Agric. Food Chem.* **2010**, *58*, 12847−12857.
(55) Martínez-Sanz, M.; Lopez-Rubio, A.; Lagaron, J. M. Optimization of the Dispersion of Unmodified Bacterial Cellulose Nanowhiskers into Polylactide via Melt Compounding to Significantly Enhance Barrier and Mechanical Properties. *Biomacromolecules* **2012**, *13*, 3887−3899.
(56) Kim, S.; Jinschek, J. R.; Chen, H.; Sholl, D. S.; Marand, E. Scalable Fabrication of Carbon Nanotube/Polymer Nanocomposite Membranes for High Flux Gas Transport. *Nano Lett.* **2007**, *7*, 2806−2811.
(57) Ma, H.; Burger, C.; Hsiao, B. S.; Chu, B. Highly Permeable Polymer Membranes Containing Directed Channels for Water Purification. *ACS Macro Lett.* **2012**, *1*, 723−726.
(58) Bhatia, A.; Gupta, R.; Bhattacharya, S.; Choi, H. Effect of Clay on Thermal, Mechanical and Gas Barrier Properties of Biodegradable Poly(lactic acid)/Poly(butylene succinate) (PLA/PBS) Nanocomposites. *Int. Polym. Process* **2010**, *25*, 5−14.
(59) Di Lorenzo, M. L.; Rubino, P.; Cocca, M. Miscibility and Properties of Poly(L-lactic acid)/Poly(butylene terephthalate) Blends. *Eur. Polym. J.* **2013**, *49*, 3309−3317.
(60) Ojijo, V.; Ray, S. S.; Sadiku, R. Effect of Nanoclay Loading on the Thermal and Mechanical Properties of Biodegradable Polylactide/Poly[(butylene succinate)-co-adipate] Blend Composites. *ACS Appl. Mater. Interfaces* **2012**, *4*, 2395−2405.
(61) Svagan, A. J.; Åkesson, A.; Cárdenas, M.; Bulut, S.; Knudsen, J. C.; Risbo, J.; Plackett, D. Cellulose Nanocomposite Biopolymer Foam—Hierarchical Structure Effects on Energy Absorption. *Biomacromolecules* **2012**, *13*, 397−405.
(62) Wu, L. L.; Wang, J. j.; He, X.; Zhang, T.; Sun, H. Using Graphene Oxide to Enhance the Barrier Properties of Poly(lactic acid) Film. *Packag. Technol. Sci.* **2014**, *27*, 693−700.
(63) Sanchez-Garcia, M. D.; Lagaron, J. M. On the Use of Plant Cellulose Nanowhiskers to Enhance the Barrier Properties of Polylactic Acid. *Cellulose* **2010**, *17*, 987−1004.
(64) Sanchez-Garcia, M.; Gimenez, E.; Lagarón, J. M. Morphology and Barrier Properties of Solvent Cast Composites of Thermoplastic

DOI: 10.1021/acsami.5b00294
ACS Appl. Mater. Interfaces 2015, 7, 8023−8032

Biopolymers and Purified Cellulose Fibers. *Carbohydr. Polym.* **2008**, *71*, 235−244.
(65) Bitinis, N.; Verdejo, R.; Maya, E.; Espuche, E.; Cassagnau, P.; Lopez-Manchado, M. Physicochemical Properties of Organoclay Filled Polylactic Acid/Natural Rubber Blend Bionanocomposites. *Compos. Sci. Technol.* **2012**, *72*, 305−313.
(66) Brenckle, M. A.; Partlow, B.; Tao, H.; Kaplan, D. L.; Omenetto, F. G. Interface Control of Semicrystalline Biopolymer Films through Thermal Reflow. *Biomacromolecules* **2013**, *14*, 2189−2195.
(67) Chang, J. H.; An, Y. U.; Sur, G. S. Poly(lactic acid) Nanocomposites with Various Organoclays. I. Thermomechanical Properties, Morphology, and Gas Permeability. *J. Polym. Sci., Part B: Polym. Phys.* **2003**, *41*, 94−103.
(68) Lange, J.; Wyser, Y. Recent Innovations in Barrier Technologies for Plastic Packaging—A Review. *Packag. Technol. Sci.* **2003**, *16*, 149−158.
(69) Xu, H.; Wu, D.; Yang, X.; Xie, L.; Hakkarainen, M. Thermostable and Impermeable "Nano-Barrier Walls" Constructured by Poly(lacitc acid) Stereocomplex Crystal Decorated Graphene Oxide Nanosheets. *Macromolecules* **2015**, DOI: 10.1021/ma502603j.

DOI: 10.1021/acsami.5b00294
ACS Appl. Mater. Interfaces 2015, 7, 8023−8032